


ARTICLE

## Application of Seismic Frequency Resonance Technology for Karst Detection at Qingshuitang Wollastonite Mining Area of Hezhou, South China

Xiaoli Gou <sup>1,2</sup>, Shehong Li <sup>1</sup>, He Yu <sup>1,2\*</sup> , Xuhong Zhou <sup>3</sup>, Hui Zhou <sup>4</sup>, Guang He <sup>5</sup>, Shangsong Han <sup>2</sup>, Chunmei Li <sup>2</sup>, Wenjiang Luo <sup>1</sup>, Zhiying Mu <sup>1</sup>, Mingyu Lu <sup>1</sup>

<sup>1</sup>College of Earth Sciences, Guilin University of Technology, Guilin 541006, China

<sup>2</sup>School of Architecture and Electrical Engineering, Hezhou University, Hezhou 542899, China

<sup>3</sup>Guangxi Hualan Rock Mechanics Engineering Co., Ltd., Nanning 530023, China

<sup>4</sup>College of Architecture and Civil Engineering, Nanning University, Nanning 530200, China

<sup>5</sup>No.204 Geological Team of Guangxi Zhuang Autonomous Region, Hezhou 542800, China

### ABSTRACT

Karst caves are among the most common and critical geological hazards in karst regions. Due to their marked differences in physical properties compared to the surrounding rock, they can be detected using various geophysical techniques. Karsts have developed on the surface of the Qingshuitang Wollastonite Mining Area in Huangtian Town, Hezhou City, Guangxi Province. In line with mine safety production requirements, a professional assessment of the potential development of karst caves must be conducted within 150 m of the mining area's surface. Following an on-site investigation and comparison with traditional geophysical methods, seismic frequency resonance technology (Seismic FRT) was selected for detection due to its convenience, flexibility, cost-effectiveness, and rapid data acquisition capabilities. Contour maps of the apparent wave impedance and geological profiles along the survey lines were obtained through data collection and processing. In combination with surface karst and mining geology, 32 karst caves (hidden danger points) and 15 karst development zones were identified. Drilling verification was conducted at the A428 and B122 anomalous points on the A1 # and B1 # survey lines. The verification results were consistent with the inferred depths and maximum apparent wave impedance anomalies, confirming that Seismic FRT is a feasible and effective method for detecting hidden karst development areas in mines.

**Keywords:** Karst; Seismic Frequency Resonance Technology; Abnormal Wave Impedance; Drilling Verification; Hezhou

#### \*CORRESPONDING AUTHOR:

He Yu, School of Architecture and Electrical Engineering, Hezhou University, Hezhou 542899, China; Email: [yuhe@hzxy.edu.cn](mailto:yuhe@hzxy.edu.cn)

#### ARTICLE INFO

Received: 7 April 2025 | Revised: 15 May 2025 | Accepted: 21 May 2025 | Published Online: 13 June 2025

DOI: <https://doi.org/10.30564/jees.v7i6.9407>

#### CITATION

Gou, X., Li, S., Yu, H., et al., 2025. Application of Seismic Frequency Resonance Technology for Karst Detection at Qingshuitang Wollastonite Mining Area of Hezhou, South China. *Journal of Environmental & Earth Sciences*. 7(6): 426–438. DOI: <https://doi.org/10.30564/jees.v7i6.9407>

#### COPYRIGHT

Copyright © 2025 by the author(s). Published by Bilingual Publishing Group. This is an open access article under the Creative Commons Attribution-NonCommercial 4.0 International (CC BY-NC 4.0) License (<https://creativecommons.org/licenses/by-nc/4.0/>).

# 1. Introduction

Karst caves are among the most common and critical hazards encountered in engineering construction in karst areas. They vary in scale and shape, but all share certain characteristics, such as significant differences in physical properties between the caves and the surrounding rock <sup>[1]</sup>. To detect karst caves, methods such as transient electromagnetic, high-density electrical, direct current depth measurements, and geological radar have been employed <sup>[1–13]</sup>. Each of these methods has its own advantages and disadvantages and is significantly influenced by the terrain.

To meet the demands of modern geophysical technology, a new seismic wave-frequency resonance exploration technology (Seismic FRT), based on large-scale computer technology, has been developed in recent years. This technology offers extremely high exploration sensitivity—particularly for medium and shallow layers—outstanding ability to distinguish geological properties, and excellent adaptability to the complex surface and subsurface environments. It relies on the seismic noise amplitude spectra at different frequencies to assess the geometric and attribute characteristics of geological bodies at various subsurface depths <sup>[14]</sup>. Seismic FRT has been successfully applied in a range of engineering practices, including deep-buried coal seam goaf areas <sup>[15,16]</sup>, the movement characteristics of overlying rocks in coal mining working faces <sup>[17]</sup>, the investigation of urban hidden active faults <sup>[14]</sup>, fault structure analysis, and geothermal prospecting <sup>[18]</sup>. It has also been used in hydraulic fracturing monitoring of coal seam roofs and deep orebody prediction in lead-zinc mining areas <sup>[19,20]</sup>.

Karsts have developed on the surface of the Qingshuitang Wollastonite Mining Area in Huangtian Town, Hezhou City, Guangxi Province. In accordance with mine safety production design requirements, a professional evaluation of the potential development of karst caves must be conducted within 150 m of the mining area's surface, including assessments of their depth, height, and width. The required construction period was 15 days. Following on-site research, Seismic FRT was selected for detection due to its convenience, flexibility, cost-effectiveness, and rapid

data collection capabilities, and it yielded satisfactory results in its application.

## 2. Geological and Karst Characteristics of the Mining Area

### 2.1. Natural Geography

The study area was the Qingshuitang Wollastonite Mining Area in Huangtian Town, Hezhou City, Guangxi Province, situated in Qingshuitang Natural Village, which is 11 kilometers away from Hezhou City at a direction of 31°. The terrain of the mining area is hilly, with the northern part being higher and the southern part lower (**Figure 1**). The minimum elevation is 130 m, the maximum elevation is 330 m, and the maximum elevation difference is 200 m. There is no major surface runoff in the area, and the surface vegetation is primarily composed of dense trees with relatively well-developed growth (**Figure 1a**). due to open-pit mining, several rocks are exposed at the bedrock surface (**Figure 1b**), leaving areas without soil. Additionally, the dominant plant species in the mining area is Quanmu, which is typically short, though it can be dense and difficult to navigate in certain areas (**Figure 1c**). This lack of soil may affect the placement of geophysical survey points, especially for conventional high-density electrical methods, where electrodes cannot be installed in bedrock areas.

### 2.2. Geology of Mining Area

The mining area (**Figure 2**) is located in the transition between the Yangtze and South China plates (**Figure 2a**), along the northeast edge of the Dayao Mountains uplift of the central northeast Guangxi fold system in the South China active belt of the South China plate, and the exposed strata include: Sinian (Z), Cambrian (C), Devonian (D), Carboniferous (C), Jurassic (J), and Quaternary (Q) deposits. This area has undergone multiple tectonic magmatic activities, forming tin, tungsten, gold, silver, lead, zinc, arsenic, sulfur, rare earth elements, marble, granite, and wollastonite.



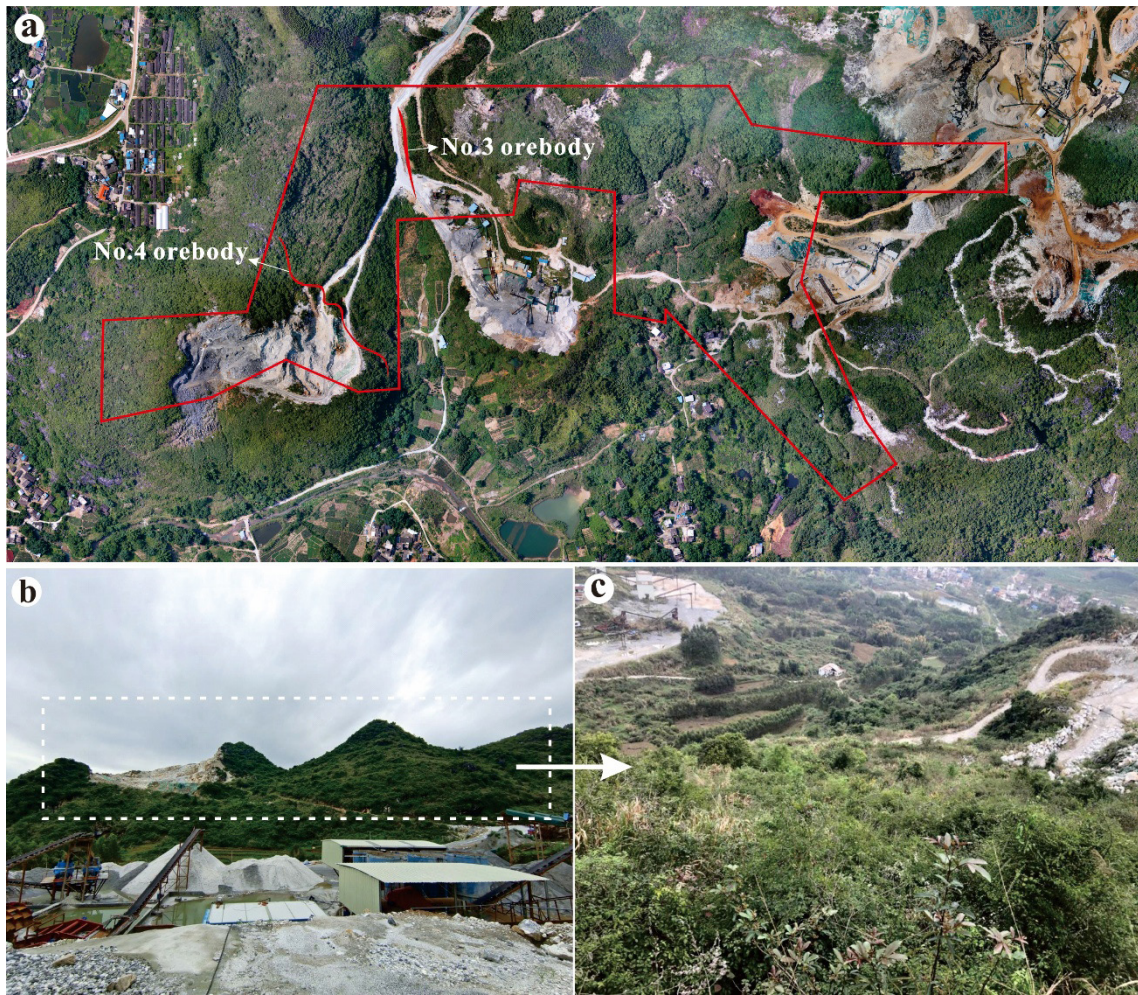


**Figure 1.** Topography and Landforms of the Mining Area. (a) Topography and Landforms of the Mining Area (Aerial Photography by Drone, with the Red Line Indicating the Entire Mining Area); (b) Surface Vegetation on the Upper Part of the No. 3 and No. 4 Orebodies; (c) Vegetation in the Northwest of the Upper Mining Area of the No. 4 Orebody.

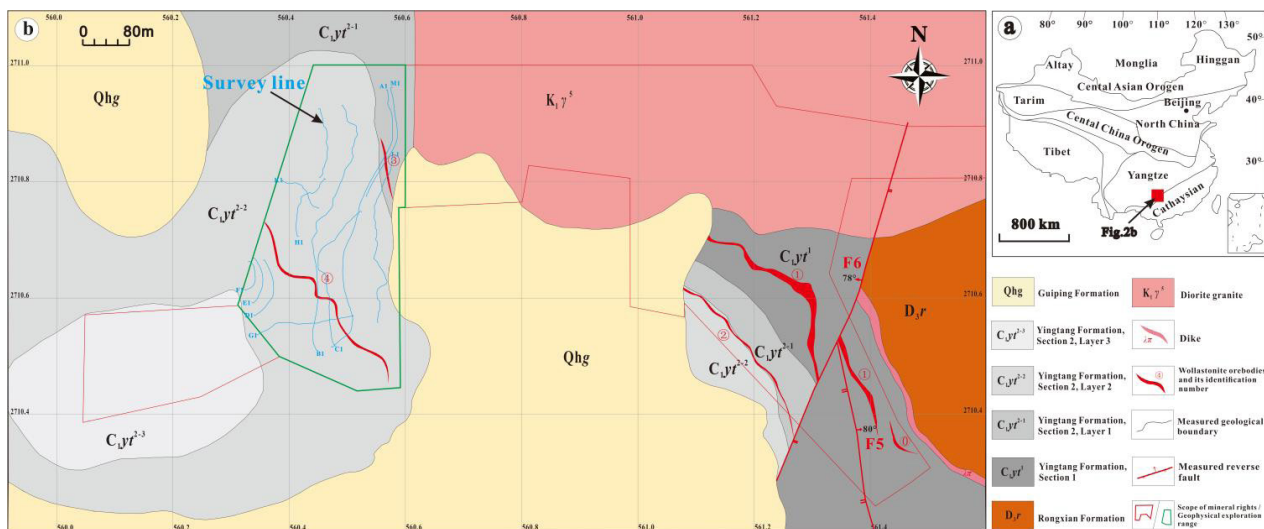


**Figure 2.** Geological Map of the Mining Area. (a) Geotectonic sketch map of China. (b) Geological sketch and Survey line map of the Ming Area.



The current mining object in the Qingshuitang mining area is wollastonite, with a total ore volume of 1.86 million tons and a mineral volume of 1.15 million tons. The wollastonite orebody is located in the middle and lower parts of the Lower Carboniferous Yingtang Formation ( $C_{1yt}$ ), in the contact zone with the Guposhan granite body. Multiple ore bodies have been developed, five of which have been identified as having industrial value (**Figure 2b**): No.0, No.1, No.2, No.3, and No.4 (**Figure 2**). The upper parts of orebodies No. 0 and No. 1 (above elevation 150 m) and orebody No. 4 are mined open-pits, whereas

the lower parts of orebody No. 1 (below elevation 150 m), No.2, and No.3 are all mined underground. In addition, two types of ore bodies were discovered through exploration on the west side of the mining area, with the industrial use of marble for powder (orebody I) and limestone for building stone (orebody I). These orebodies have not yet been mined or utilized. The density measurement (**Table 1**) shows the range of density variation for wollastonite, marble, limestone and granite. Overall, the density of the wollastonite orebody is higher than that of the surrounding rock, reflecting its high wave impedance characteristics.

**Table 1.** Density Parameter Measurement Results in the Mining Area.

No.	Rock and Ore Name	Sample Quantity (pieces)	Density $\rho$ (g/cm <sup>3</sup> )		Remarks
			Change Range	Average Value	
1	Wollastonite	20	2.75–2.91	2.80	Fibrous, columnar ore
2	marble	30	2.69–2.92	2.75	Powder with marble ore or surrounding rock
3	Limestone	30	2.65–2.76	2.72	Limestone ore for building stones or surrounding rock
4	Granite	30	2.58–2.63	2.61	surrounding rock

The exposed strata in the mining area, from old to new, include the Late Paleozoic Lower Carboniferous Yingtang ( $C_{1yt}$ ) Formation and the Cenozoic Guiping Formation (Qhg).  $C_{1yt}$  is distributed along the eastern and western sides of the mining area, with a northwest–southeast orientation. The mineralization and ore-bearing layer in this area consists primarily of light gray–white to white marble and light gray–black limestone. Based on geological survey results,  $C_{1yt}$  has been divided into two lithological sections, from bottom to top: Yingtang Formation Sections 1 ( $C_{1yt}^1$ ) and 2 ( $C_{1yt}^2$ ).  $C_{1yt}^2$  is further divided into three lithological layers from bottom to top, namely Yingtang Formation Section 2 Layers 1 ( $C_{1yt}^{2-1}$ ), 2 ( $C_{1yt}^{2-2}$ ), and 3 ( $C_{1yt}^{2-3}$ ), as shown in **Figure 3**.

Geological strata in mining areas are influenced by structures, resulting in significant changes in their occurrence. The western strata have a dip direction of 225–270° and a dip angle of 25–50°, whereas the eastern strata have a dip direction of 217–255° and a dip angle of 40–53°. The No.4 orebody is exposed in the western part of the mining area and is located in the upper part of  $C_{1yt}^{2-2}$ . The orebody has a northwest strike, length of 440 m, dip depth of more than 50 m, thickness of 3.2–4.8 m, and an average thickness of 4.1 m.

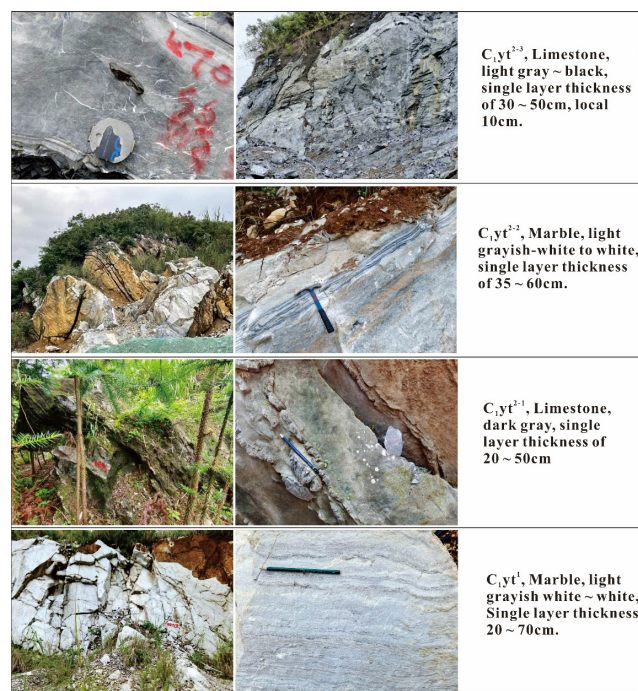


**Figure 3.** Characteristics of Ore Bearing Strata in the Mining Area.

Magmatic rocks are distributed in the northern part of the mining area (**Figure 2a**) and are part of the Guposhan rock mass ( $K_1\gamma^5$ ). The rock mass is planar in shape, with an exposed area exceeding 13 km<sup>2</sup>. Surface weathering is significant, and the weathering layer is relatively thick in

certain areas. The rock mass in the northwest of the mining area is surrounded by  $C_1vt^{-1}$ , and its lithology consists of dark gray chert containing banded limestone, with a fault contact between the two. In the central part of the mining area, the surrounding rock is also  $C_1vt^{-1}$ , and the lithology is light gray-white to white banded marble with two intrusive contacts. The contact metamorphic zone between the magmatic rock mass and the  $C_1vt$  strata is a favorable location for the development of both orebodies and wollastonite orebodies.

### 2.3. Surface Karst Characteristics

The mining area and surrounding terrain are characterized by hilly landforms, with exposed bedrock and surface rock dissolution. The mountain surfaces feature karst gullies, troughs, and fissures, and small karst caves are locally developed along the slopes. The length and width of a single development groove or trough range from 0.5 to 2.0 m, 0.2 to 20.5 m, and 0.5 to 1.5 m, forming a “V” shape. Karst fissures often develop along the rock layers or joint surfaces, opening at the surface and closing at depth, partially filled

with gray matter. The diameter of the caves ranges from 0.5 to 1.5 m, with varying depths. Four observation points with exposed bedrock and karst development were selected within the mining area for a survey and data statistics of surface karst rates. According to the survey, the surface rock rates at the four observation points were 13.67%, 7.42%, 9.2–3%, and 6.93%, respectively, with an average surface karst rate of 6.33% (**Table 2**). The survey results indicate that surface karst is well-developed in the mining area.

### 2.4. Geophysical Characteristics

The resonant apparent wave impedance gradually increased from the cover layer to the bedrock. When loose underground soil, cracks, and cavities were encountered, the resulting resonant map showed relatively low apparent wave impedance. Significant differences in apparent wave impedance were observed among the karst caves, loose soil, cover layers, and bedrock, making them well-suited for geophysical exploration. The differences in the physical properties of the various layers at the site are listed in **Table 3**.

**Table 2.** Statistics of Surface Karst Rate.

No.	Survey Area (m <sup>2</sup> )	Karst Surface (m <sup>2</sup> )	Surface Karst Rate (%)	Average Rock Ratio in the Mining Area (%)
YR1	300	41.01	13.67	6.33
YR2	120	8.9	7.42	
YR3	120	11.97	9.98	
YR4	120	8.31	6.93	
total	660	70.19	10.63	

**Table 3.** Range Values of Physical Property Layer Parameters in the Measurement Area.

Physical property layer	Clay	Bedrock	Loose Soil, Cracks, and Caves
Visual impedance (g/m <sup>3</sup> m/s)	300–1100	>1350	300–1100

## 3. Methods

Seismic FRT is a frequency-domain passive source seismic exploration method <sup>[21]</sup>, which has been applied in urban geological exploration, resource exploration, disaster geological exploration, and deep earth geological research <sup>[12,14,16,17,22–23]</sup>. This method has a large detection depth, high accuracy, fast construction efficiency, and low cost. Furthermore, it is not affected by the electromagnetic environment and has no destructive impact on the surrounding environment.

### 3.1. Method Principle

Natural frequency is an intrinsic property of an object and every object has its own natural frequency, including the underground medium. When subjected to vibration, if the vibration frequency matches its natural frequency, the medium experiences self-excited resonance, amplifying the amplitude of the external input vibration.

Seismic waves also exhibit resonance characteristics, and Seismic-FRT leverages this resonance principle to

obtain the geometric and attribute characteristics of geological bodies at different depths. This is achieved through natural noise acquisition, processing, and imaging to detect underground media <sup>[21,24]</sup>. The basic principles are as follows:

The wave field resonates with the geological body during its propagation from the underground to the ground. Then the amplitude spectrum,  $W_{(c,f)}$ , of the resonant field tuned by the Earth can be written as

$$W_{(c,f)} = In(f) \times M_{(c,f)}, \quad (1)$$

where  $M_{(c,f)}$  is the transfer function,  $In(f)$  is the excitation field function,  $C$  is a function related to the geological parameters, and  $F$  is the signal frequency. The expression is an amplifier formula for frequency-domain filtering.

Assuming that the excitation source field,  $In(f)$ , is a plane wave, to obtain the parameters of the underground medium in the target area, Equation (1) can be rewritten as:

$$M_{(c,f)} = W_{(c,f)} \div In(f), \quad (2)$$

The theoretical formula for magnification is:

$$M(\text{theory}) \propto \frac{1}{\left[ \cos^2(\theta) + \Omega_1/\Omega_2 \times \sin^2(\theta) \right]}, \quad (3)$$

Where  $\theta$  is the angle between the underground wavefield and the level ground ( $^\circ$ );  $\Omega_1$  is the upper layer wave impedance value ( $\text{g/m}^3 \cdot \text{m/s}$ ); and  $\Omega_2$  is the impedance value of the lower layer wave ( $\text{g/m}^3 \cdot \text{m/s}$ ).

When  $\theta = 90^\circ$ , resonance occurs, and the noise amplitude spectrum measured on the ground is a statistical understanding of resonance products. At this point,  $M_{(\text{theory})}$  is only a function of  $\Omega_1$  and  $\Omega_2$ , that is:

$$M(\text{theory}) \propto \frac{1}{\left[ \Omega_2/\Omega_1 \right]}, \quad (4)$$

The above equation indicates that there is a definite expression for the amplification function and a two-series equation for formation. When an amplification factor (transfer function) exists, the formation parameters can be calculated as follows: Using a first-order approximation, we obtain

$$\Omega_1' / \Omega_2' = W_{(c,f)} / In(f), \quad (5)$$

Where  $\Omega_1'$  is the upper layer wave impedance value after

the first-order approximation ( $\text{g/m}^3 \cdot \text{m/s}$ ), and  $\Omega_2'$  is the lower layer wave impedance value after the first level ( $\text{g/m}^3 \cdot \text{m/s}$ ).

Thus, different ground wave impedance ratios of underground media can be obtained, and geological information, such as wave impedance parameters or density, can be inverted, ultimately revealing the spatial characteristics of underground geology.

### 3.2. Data Collection

Based on the characteristics of Seismic FRT and the terrain and geomorphic conditions of the mining area, 12 three-line profiles (non-straight lines, which do not impact data processing or analysis) were deployed over orebodies No. 3 and No. 4 (**Figure 2b**). The survey had a detection point distance of 5 m, a sampling window of 300 s, 611 measurement points, a total length of 2990 m, and a detection depth of 150 m. For field data collection, a wireless digital portable seismic frequency resonance acquisition station (model FRT-IMG-III), with a working frequency range of 0.05–150 Hz and a sampling rate of 100 Hz, was used. Natural seismic resonance signals were collected point by point along the profile using a single point, single station approach, and RTK was employed to determine the position of each measurement point with centimeter-level accuracy.

Before the start of fieldwork, consistency tests were conducted on all instruments to ensure unified exploration accuracy across the entire area. Data collection stations with consistency indicators between 0.9 and 1.1 were selected. The results of the consistency tests are presented in **Table 4**. The test results showed that the various indicators of the instruments were normal and consistent, and the data collection process remained stable throughout the work, thus meeting the project's technical requirements for the instruments.

**Table 4.** Results of the Consistency Test.

Instrument Number	Consistency Test				
	X_ever	Y_ever	Z_ever	XY_ever	Tot_ever
1	1.01305	1.00386	1.03264	1.00846	1.03025
2	0.990048	0.977176	1.01076	0.978612	0.995376
3	0.950369	0.993041	0.982751	0.971705	0.997164
4	0.984784	0.998144	0.965077	0.981464	0.972522

Table 4. Cont.

Instrument Number	Consistency Test				
	X_ever	Y_ever	Z_ever	XY_ever	Tot_ever
5	1.0076	1.02253	0.987037	1.03007	1.0073
6	0.990892	0.995906	0.980728	0.978399	0.973069
7	0.972659	1.02216	0.971236	0.997409	0.983287
8	1.01449	0.997203	1.02946	1.00585	1.01938

After the fieldwork was completed, the relevant earthquake wave data were copied, the corresponding point data for each corresponding time was intercepted, and the data was checked and uploaded to the cloud disk for backup to ensure data security. During the inspection, any non-conforming data were recollected to ensure the accuracy and reliability of the raw data.

### 3.3. Data Processing

Seismic FRT utilizes the correlation between the amplitude of the vibration field after transverse wave (S-wave) resonance and the impedance changes of the underground medium to image geological bodies at specific depths. The location, impedance ratio, or impedance value of the underground medium can be determined based on the resonant frequency. The contents and processes are as follows:

- ① The response signals of the underground medium collected in the field form seismic time series data.
- ② The collected seismic time-series data were filtered.
- ③ After processing the data through wavefield analysis, frequency-domain data were formed through a Fourier transform.
- ④ Each component of frequency domain data was overlain multiple times to obtain multiple superimposed data.
- ⑤ Noise suppression and smoothing were performed on the superimposed frequency domain data.
- ⑥ Resonance selection and in-depth analysis were performed on frequency domain data, removing random frequency components and highlighting tuning frequencies.
- ⑦ The resonant wave impedance of the formation was inverted to obtain the transverse wave (S-wave) im-

pedance ratio of the detection profile.

## 4. Results

The impedance value of rock waves is the product of the rock density at 2°C and velocity <sup>[25]</sup>; the velocity is generally positively correlated with density <sup>[26]</sup>. Therefore, the impedance characteristics of geological bodies reflect their density characteristics. The strata and main rock types in the mining area include Quaternary humus soil and residual slope deposits, of the Lower Carboniferous Yingtang Formation marble, limestone, and wollastonite, and Cretaceous fine-grained diorite. The strata and rock types in this exploration area primarily consist of the first two.

The density of marble and limestone in the survey area is relatively high, resulting in high wave impedance characteristics, while caves, rock fracture zones, and pores exhibit relatively low wave impedance characteristics. Based on the analysis of the density-wave impedance relationship for various rock types, geological information can be interpreted from the resulting map of the seismic frequency resonance exploration, specifically the contour map of the apparent wave impedance along the survey line. Data collection and processing for 12 survey lines into maps took only ten days, making this method significantly more efficient than traditional geophysical techniques. Through experiments and similar engineering experiences, adverse geological bodies such as loose soil, cracks, and caves exhibited significant reactions in the Seismic FRT wave impedance results map. On the cross-sectional image map, these appear as low-impedance closed circles or contour lines with distinct concave shapes against the background. In general, the apparent wave impedance is less than 1/4 of the background value. Combined with known geological tunnel data, this area is identified as a geophysical anomaly zone. The statistical results of the frequency-resonance anomalies are listed in **Table 5**. The speculated caves (hidden danger points) are mainly distributed on lines A1 #, B1 #, C1 #, D1 #, E1 #, J1 #, L1 #, and M1 #, 32 in total. The karst development zones are mainly distributed on lines A1 #, B1 #, D1 #, F1 #, G1 #, H1 #, J1 #, and M1 #, 15 in total.



**Table 5.** Statistics of Frequency Resonance Anomalies.

N0.	Exception Number	Measurement Line	Starting Point Position (m)	Endpoint Position (m)	Abnormal Length (m)	Abnormal Top Burial Depth (m)	Abnormal Bottom Burial Depth (m)	Abnormal Height (m)	Exception Type
1	AR1	A1#	46.4	70.6	24.2	32.5	38.8	6.3	Cave (hidden danger point)
2	AR2		219.6	232.8	13.2	15.5	20.3	4.8	Cave (hidden danger point)
3	AR3		259.6	272.0	12.4	16.3	28.4	12.1	Cave (hidden danger point)
4	AR4		357.9	365.3	7.4	17.2	25.2	8.0	Cave (hidden danger point)
5	AR5		468.9	475.3	6.4	18.5	24.3	5.8	Cave (hidden danger point)
6	BR1	B1#	111.9	118.8	6.9	36.0	41.2	5.2	Cave (hidden danger point)
7	BR2		300.3	307.8	7.5	18.4	23.6	5.2	Cave (hidden danger point)
8	BR3		102.8	112.5	9.7	153.8	158.9	5.1	Cave (hidden danger point)
9	BR4		147.8	152.8	5	125.6	130.2	4.6	Cave (hidden danger point)
10	BR5		177.3	188.0	10.7	120.1	123.4	3.3	Cave (hidden danger point)
11	BR6		218.3	225.3	7	120.5	129.1	8.6	Cave (hidden danger point)
12	BR7		457.4	465.3	7.9	113.0	119.2	6.2	Cave (hidden danger point)
13	CR1	C1#	66.0	74.7	8.7	27.9	32.3	4.4	Cave (hidden danger point)
14	CR2		123.7	136.2	12.5	28.3	39.6	11.3	Cave (hidden danger point)
15	CR3		217.5	227.4	9.9	18.0	23.1	5.1	Cave (hidden danger point)
16	CR4		282.9	291.5	8.6	28.3	33.4	5.1	Cave (hidden danger point)
17	DR1	D1#	67.1	71.8	4.7	11.9	17.6	5.7	Cave (hidden danger point)
18	DR2		151.9	156.5	4.6	10.0	12.7	2.7	Cave (hidden danger point)
19	ER1	E1#	59.6	64.6	5	6.6	9.9	3.3	Cave (hidden danger point)
20	JR1	J1#	15.2	19.7	4.5	12.2	14.8	2.6	Cave (hidden danger point)
21	JR2		41.8	44.1	2.3	19.2	23.2	4.0	Cave (hidden danger point)
22	JR3	J1#	69.9	72.5	2.6	52.4	54.0	1.6	Cave (hidden danger point)
23	JR4		51.7	59.3	7.6	140.2	151.3	11.1	Cave (hidden danger point)
24	LR1	L1#	14.0	18.9	4.9	38.7	46.2	7.5	Cave (hidden danger point)
25	LR2		73.5	82.3	8.8	44.0	50.8	6.8	Cave (hidden danger point)
26	LR3		133.8	137.9	4.1	16.1	21.2	5.1	Cave (hidden danger point)
27	LR4		269.2	273.0	3.8	32.9	34.9	2.0	Cave (hidden danger point)
28	LR5		328.1	332.7	4.6	23.9	26.3	2.4	Cave (hidden danger point)
29	MR1	M1#	73.7	81.7	8	21.7	26.9	5.2	Cave (hidden danger point)
30	MR2		159.9	166.1	6.2	15.5	19.1	3.6	Cave (hidden danger point)
31	MR3		194.9	203.1	8.2	15.2	20.7	5.5	Cave (hidden danger point)
32	MR4		52.9	56.8	3.9	157.7	162.9	5.2	Cave (hidden danger point)
33	A1	A1#	227.2	246.7	19.5	117.8	134.1	16.3	Karst development zone
34	A2		324.5	353.9	29.4	102.9	115.7	12.8	Karst development zone
35	A3		463.5	482.9	19.4	158.3	192.4	34.1	Karst development zone
36	B1	B1#	227.5	264.3	36.8	54.5	66.1	11.6	Karst development zone
37	D1	D1#	16.6	24.6	8	20.1	27.5	7.4	Karst development zone
38	D2		39.9	45.2	5.3	8.0	16.9	8.9	Karst development zone
39	F1	F1#	33.0	39.7	6.7	7.0	11.2	4.2	Karst development zone
40	F2		48.9	51.9	3	15.1	18.9	3.8	Karst development zone
41	F3		92.3	95.6	3.3	9.7	13.4	3.7	Karst development zone
42	G1	G1#	56.0	69.3	13.3	13.8	20.7	6.9	Karst development zone
43	H1	H1#	112.4	124.4	12	13.3	26.2	12.9	Karst development zone
44	H2		64.9	73.6	8.7	159.3	167.5	8.2	Karst development zone
45	J1	J1#	45.6	56.1	10.5	78.9	92.0	13.1	Karst development zone
46	J2		100.1	110.7	10.6	93.4	105.4	12.0	Karst development zone
47	M1	M1#	88.3	97.1	8.8	96.6	104.8	8.2	Karst development zone



The contour maps of the apparent wave impedance for measurement lines A1 # and B1 # are examples of interpretation and explanation, respectively. **Figure 4** shows that the apparent wave impedance ratio of the A1 # measuring line is less than 1200 at the horizontal positions of 46.4–70.6, 219.6–232.8, 259.6–272.0, 357.9–365.3, and 468.9–475.3 m, indicating a closed loop of the apparent wave impedance anomaly. This is an abnormal point in the karst cave (hidden danger point). At the horizontal positions of 227.2–246.7, 324.5–353.9, and 463.5–482.9 m, there is a concave apparent low wave impedance anomaly, which is speculated to be a karst development zone. The inferred geological profile of the A1 # survey line (**Figure 5**) shows that the karst cave is circular, elliptical, and horizontally strip-shaped, with an area of 29.3–118.6 m<sup>2</sup>, vertical depth distribution of 15.5–38.8 m below the surface, and elevation of 183.4–130.3 m. The karst development zone is horizontally elongated, water droplet-shaped, and elliptical, with an area of 231.1–512.1 m<sup>2</sup>, vertical depth distribution of 102.9–192.4 m below the surface, and elevation of 81.410.5 m.

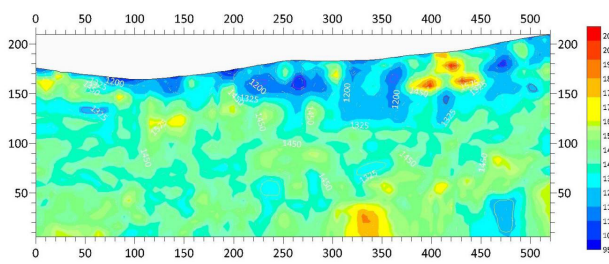


**Figure 4.** A1 # Line Apparent Wave Impedance Contour Map (Scale 1:1000, Unit: meters, the Vertical Coordinate Represents Depth, and the Horizontal Coordinate Represents Distance).

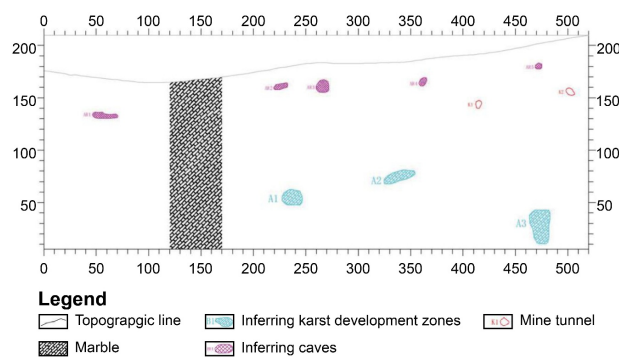


**Figure 5.** A1 # Geological Profile Inferred from Survey Line (Scale 1:1000, Unit: meters, the Vertical Coordinate Represents Depth, and the Horizontal Coordinate Represents Distance).

**Figure 6** shows that the apparent wave impedance

ratio of the B1 # survey line is less than 1200 at horizontal positions 111.9–118.8, 300.3–307.8, 102.8–112.5, 147.8–152.8, 177.3–188.0, 218.3–225.3, and 457.4–465.3 m. The apparent wave impedance anomaly appears as a closed loop and is an abnormal point in the karst cave (hidden danger point). At the horizontal position of 227.5–264.3 m, there is a concave apparent low wave impedance anomaly, which is a karst development zone. The inferred geological profile of the B1 # survey line (**Figure 7**) exhibits circular, elliptical, and quasi-elliptical shapes with an area of 18.3–42.2 m<sup>2</sup>, a vertical depth distribution of 18.3–153.8 m below the surface, and an elevation of 53.3–191.2 m. The development zone of Rock 2 is elliptical in shape, with an area of 421.8 m<sup>2</sup> and vertical depth distribution of 54. m below the surface, at an elevation of 155.0 m.

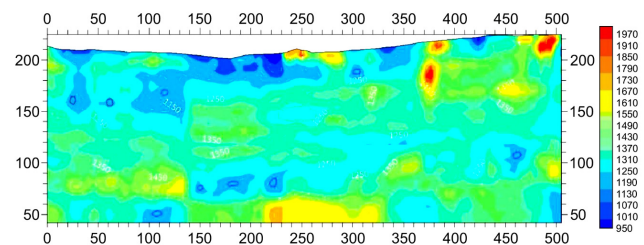


**Figure 6.** Isogram of Apparent Wave Impedance of the B1 # Survey Line (Scale 1:1000, Unit: meters, the Vertical Coordinate Represents Depth, and the Horizontal Coordinate Represents Distance).

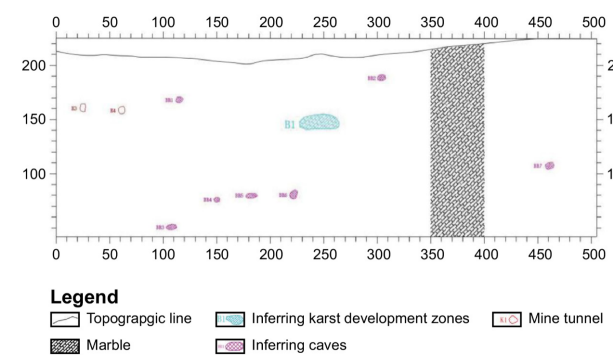


**Figure 7.** Inferred Geological Profile of the B1 # Survey Line (Scale 1:1000, Unit: meters, the Vertical Coordinate Represents Depth, and the Horizontal Coordinate Represents Distance).

## 5. Verification

To improve the accuracy of this detection, drilling verification was performed at the A428 and B122 abnormal points on the A1# and B1# survey lines based on the anomalous characteristics observed in the seismic frequen-

cy resonance wave impedance result map. This verification took into account factors such as funding, drilling site conditions, and the minimum amount of engineering required

to confirm the distribution of anomalies. Two boreholes, ZK01 and ZK02, were designed with depths of 61 and 60 m, respectively. The design parameters are listed in **Table 6**.

**Table 6.** Design Verification Drilling Results for Frequency Resonance Anomalies.

Verify Borehole Number	Exception Number	X-coordinate (2000)	Y-coordinate (2000)	Elevation (m)	Hole Depth (m)	Expected Abnormality Position (m)
ZK01	A428	2710588.081	37560498.903	186.507	61.0	23–31, 35–48
ZK02	M228	2710737.035	37560545.800	174.210	60.0	17–24, 42–48

The completed depths of ZK01 and ZK02 were 61.29 m and 99.94 m, respectively (**Figures 8 and 9**). ZK01 exhibited abnormal apparent wave impedance at depths of 23–31 m and 35–48 m below the surface, with the maximum anomaly occurring between 35.3 m and 51.4 m. ZK02 exhibited abnormal apparent wave impedance at a depth of 55–85 m below the surface, with the maximum anomaly located between 61.3 m and 64.0 m. The ZK01 drilling core (**Figure 10**) showed developed fractures at 28.6–28.7 m, with no filling material and iron infiltration along the fracture surfaces (**Figure 10a**). A cave was discovered at a depth of 40.6–42.0 m (**Figure 10b**), filled with white weathered material. The drilling core results were consistent with the inferred depth and abnormal apparent wave impedance. The skarn vein was located at 61.3–64.0 m, and quartz veins were developed at 63.14–63.17 m (**Figure 11a**), corresponding to the location of the maximum anomaly (61.3–64.0 m) (**Figure 11a**). The skarn containing quartz veins was the primary cause of the observed wave impedance anomaly. The cracks were displayed at 66.2–66.5 m (**Figure 11b**) in ZK02 drilling core, with widths of 1–2 mm, almost no filling material, and a

small amount of visible calcite crystals.

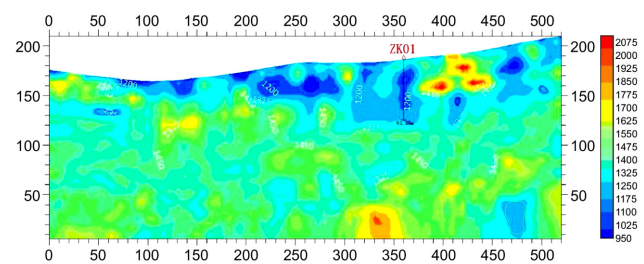


**Figure 8.** Verification of the ZK01 Borehole with Abnormal Apparent Wave Impedance on A1 # Measurement Line A428 (Scale 1:1000, Unit: meters, the vertical Coordinate Represents Depth, and the Horizontal Coordinate Represents Distance).

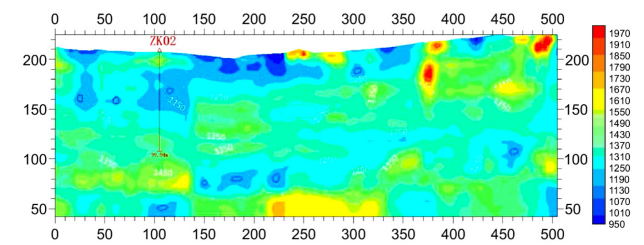


**Figure 9.** Verification of the ZK01 Borehole with Abnormal Apparent Wave Impedance on Line B122 (Scale 1:1000, Unit: meters, the Vertical Coordinate Represents Depth, and the Horizontal Coordinate Represents Distance).

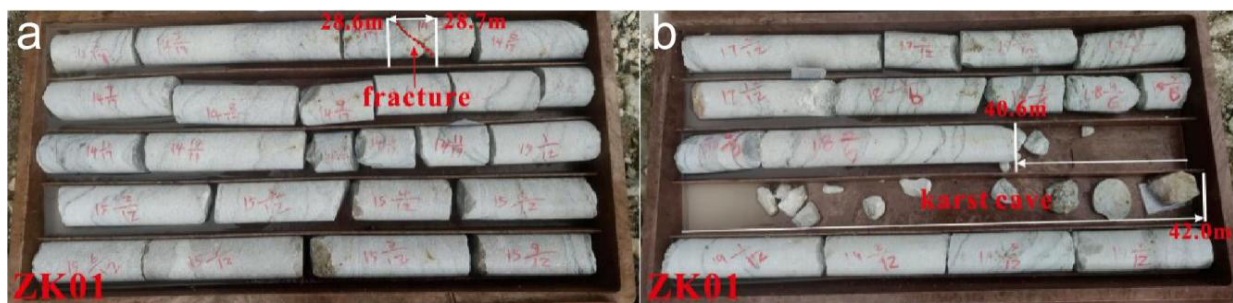


**Figure 10.** Photos of the ZK01 Drilling Core. (a) Box 6 core photos. (b) Box 8 core photos.



**Figure 11.** Photos of the ZK02 Drilling Core. (a) Box 11 core photos. (b) Box 12 core photos.

## 6. Conclusions

(1) The geological, geographical, and mining conditions of the Qingshuitang Wollastonite Mining Area in Hezhou City, Guangxi, are relatively complex, making karst development unsuitable for conventional geophysical exploration techniques. The use of Seismic FRT for detection can enhance the results while reducing data requirements.

(2) Based on the results of the Seismic FRT, 32 karst caves (hidden danger points) and 15 karst development zones were identified using a contour map of the apparent wave impedance.

(3) Drilling verification was conducted on the A428 and B122 abnormal points on the A1 # and B1 # survey lines. The verification results were consistent with the inferred depth and maximum apparent wave impedance anomalies, indicating that Seismic FRT can feasibly detect hidden karst development areas in mines.

## Author Contributions

For research articles with several authors, a short paragraph specifying their individual contributions must be provided. The following statements should be used “Conceptualization, X.G. and H.Y.; methodology, S.L.; software, X.Z; validation, G.H; formal analysis, H.Z.; investigation, S.H.,W.L., Z.M., M.L.; data curation, C.L.; writing—original draft preparation, X.G.; writing—review and editing, H.Y.; visualization, X.Z.; supervision, S.L.; project administration, X.G.; funding acquisition, H.Y. and H.Z.. All authors have read and agreed to the published version of the manuscript.” Authorship must be limited to those who have contributed substantially to the work reported.

## Funding

This work was supported by the General Project of Guangxi Natural Science Foundation grant number [2020GXNSFAA297088], the Hezhou Science Research and Development Plan Project grant number [2024143] and the Basic Research Ability Enhancement Project for Young and Middle-aged Teachers at Guangxi Universities grant number [2024KY1877].

## Institutional Review Board Statement

This study is an engineering application research based on geophysical prospecting methods to detect whether there is a karst cave below the surface of wollastonite mining area, and does not involve humans or animals.

## Informed Consent Statement

Not applicable

## Data Availability Statement

All data are included in this paper and are directly available.

## Acknowledgments

This work was financially supported by the General Project of Guangxi Natural Science Foundation (Grant No. 2020GXNSFAA297088), the Hezhou Science Research and Development Plan Project (Grant No. 2024143) and the Basic Research Ability Enhancement Project for Young and Middle-aged Teachers at Guangxi Universities (Grant No. 2024KY1877).



## Conflicts of Interest

The authors declare no conflict of interest.

## References

- [1] Han, P., 2020. Forward modeling and inversion of the high-density resistivity method in detecting karst caves of different filling types. *Geological Exploration*. 56(6), 1219–1225.
- [2] Hu, L., Huang, D.J., Xie, S.B., et al., 2022. Application Research of Comprehensive Geophysical Prospecting Techniques in Karst Cave Detection of Limestone Mines: A Case Study of Dingxiangshan Limestone Mine in Guigang City, Guangxi. *Mineral Resources and Geology*. 36, 1182–1189. [in Chinese]
- [3] Hu, H., Xue, Y., Zhang, X., 2024. Application research of three-dimensional high-density electrical method in shallow karst cave detection. *Water Resources and Hydropower News*. 45, 7–9. [in Chinese]
- [4] Huang, S., Ouyang, Y., 2009. Application of high-density electrical method in karst exploration. *Chinese Journal of Engineering Geophysics*. 6(6), 720–723.
- [5] Jiang, Y., Kang, W., Zhang, N., 2007. Application of high-density resistivity method in karst exploration. *Journal of Chengdu University of Technology (Science and Technology Edition)*. 34, 452–455.
- [6] Li, J., 2005. *Geoelectric Field and Electrical Exploration*. Geological Publishing House: Beijing, China. pp. 364.
- [7] Liu, S., 1997. A summary of the application of geophysical methods in karst exploration. *Geological Science and Technology Information*. 2, 85–91. [in Chinese]
- [8] Lu, G., Xia, J., Chen, J., 2006. Comprehensive application of high-density resistivity method and transient electromagnetic method in site karst exploration. *Geological Prospecting Collection*. 21, 6–9. [in Chinese]
- [9] Xiang, M., Chen, Y., 2004. Application of geological radar in detecting cracks in limestone caves. *Western Exploration Engineering*. 12, 155–156. [in Chinese]
- [10] Xu, H., Hu, J., Peng, Q., et al., 2017. Application of transient electromagnetic method in foundation exploration of karst areas. *Chinese Journal of Engineering Geophysics*. 14, 206–210. [in Chinese]
- [11] Xue, G.Q., Song, J.P., Ma, Y., 2003. Detecting the limestone dissolved cavern by using transient electromagnetic method. *Journal of Chang'an university (Earth Science Edition)* [in Chinese]. 25(2), 50–53.
- [12] Zhou, Z., 2019. Application of comprehensive geophysical exploration methods in geological hazard investigation of cave collapse in Qixia Zhongqiao Area. *Geology of Shandong*. 35, 47–52. [in Chinese]
- [13] Zhu, L., 2016. Application of direct current sounding method in cave exploration. *Coal Chemical Industry*. 39, 130–132. [in Chinese]
- [14] Xue, A., Li, D., Song, H., et al., 2021. Imaging of the Earth using frequency resonance effect of vibration noise. *Geological Review*. 67, 47–48. [in Chinese]
- [15] Li, X., Tian, Y., Wang, G., et al., 2023. Application and effect analysis of seismic frequency resonance technology in the “three zones” of coal mine goaf. *Shanxi Coal*. 43, 97–101. [in Chinese]
- [16] Zhu, C., Li, H., 2021. Application of seismic frequency resonance technology in the detection of deep buried coal seam goaf. *Chinese Journal of Engineering Geophysics*. 18, 774–779. [in Chinese]
- [17] Zhang, X., Xue, A., Xie, H., et al., 2021. Study on overburden movement characteristics of coal face based on frequency resonance technology. *Coal Technology*. 40, 20–22. [in Chinese]
- [18] Wang, Y., Qi, Z., Xu, G., 2023a. Application of seismic wave frequency resonance method in fault structure exploration in Jinghe County and geothermal prospect analysis. *Xinjiang Geology*. 41, 300–304. [in Chinese]
- [19] Wang, F., Tian, Y., Han, N., et al., 2023b. Application and analysis of seismic frequency resonance technology of hydraulic fracturing monitoring in roof of coal seam [in Chinese]. *China Mining Magazine* [in Chinese]. 32(12), 100–106.
- [20] Zhang, H., Zhang, G., Xue, A., et al., 2024. Application of seismic frequency resonance technology in the exploration of the Erguna Dongjun silver lead zinc mining area in Inner Mongolia [in Chinese]. *Geological Exploration* [in Chinese]. 60(2), 311–318. DOI: <https://doi.org/10.12134/j.dzykt.2024.02.008>
- [21] Xue, A. (inventor), 2019. Passive source seismic frequency resonance exploration method. State Intellectual Property Office of the People's Republic of China Patent. CN110954943A. 2019 September 5.
- [22] Li, H., Yang, J., Wang, Q., et al., 2020. Application of shallow seismic exploration combining mixed source surface waves and three-component frequency resonance method in fine detection of urban shallow geological structure. *Progress in Geophysics*. 35(3), 1149–1155. DOI: <https://doi.org/10.6038/pg2020DD0079>
- [23] Xu, J., Zhang, X., Li, X., et al., 2022. Application of shallow seismic exploration method in investigation of urban concealed active faults. *Urban Geology*. 17, 79–84. [in Chinese]
- [24] Li, H., Hou, Z., 2020. Application of seismic exploration method based on resonance principle in resource exploration [in Chinese]. *World Nonferrous Metals* [in Chinese]. 9, 159–160.
- [25] Zhang, X., 2016. Discussion on the standardiza-

- tion of wave impedance usage units [in Chinese]. Journal of Xi'an Shiyou University (Natural Science Edition) [in Chinese]. 31, 48–51. DOI: <https://doi.org/10.3969/j.issn.1673-064X.2016.03.007>
- [26] Ma, Z., Jie, J., 2005. Study on the laws of longitudinal and transverse wave velocities and density of rocks. Progress in Geophysics. 20, 905–910. [in Chinese]